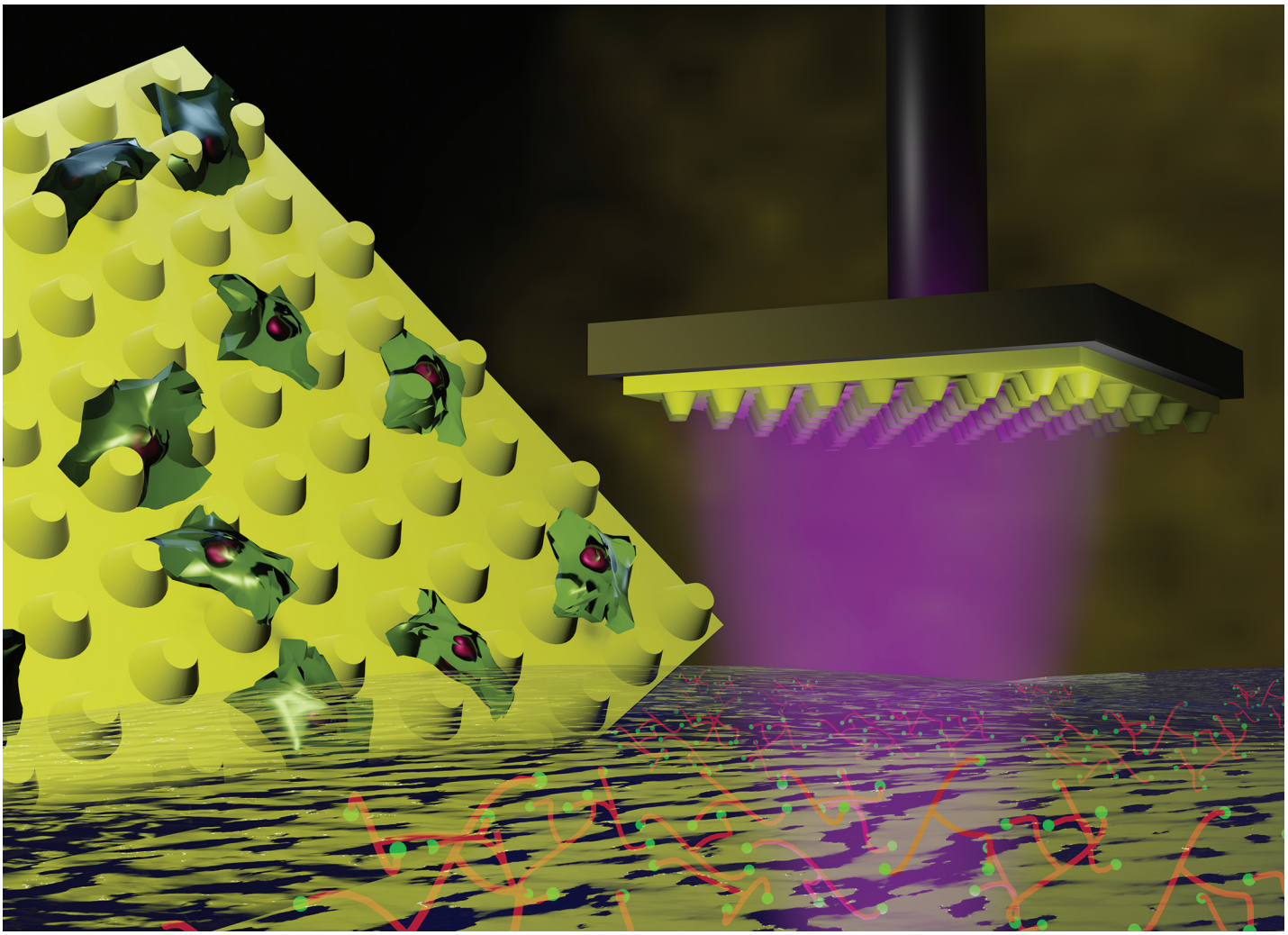

Showcasing research from Dr. Camarero-Espinosás Lab (BioSmarTE), POLYMAT, University of Basque Country UPV / EHU, Donostia / San Sebastián, Spain.

Low molecular weight poly((D,L)-lactide-*co*-caprolactone) liquid inks for diluent-free DLP printing of cell culture platforms

Sandra Ramos-Díez, Garazi Larrañaga-Jaurrieta *et al.* demonstrate the synthesis of a library of inks based on 2- and 3-arm copolymers and homopolymers. The inks present low viscosity that enables solvent-free DLP printing of high resolution and shape fidelity topographies. Biocompatibility studies highlight the potential of these inks as cell culture platforms.

As featured in:

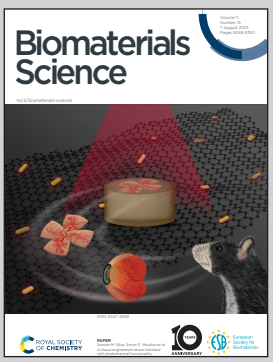

See Sandra Ramos-Díez, Garazi Larrañaga-Jaurrieta *et al.*, *Biomater. Sci.*, 2023, **11**, 5163.

ROYAL SOCIETY OF CHEMISTRY

rsc.li/biomaterials-science

Registered charity number: 207890

Biomaterials Science

ROYAL SOCIETY OF CHEMISTRY

PAPER

View Article Online
View Journal | View Issue

Cite this: *Biomater. Sci.*, 2023, **11**, 5163

Low molecular weight poly((D,L)-lactide-*co*-caprolactone) liquid inks for diluent-free DLP printing of cell culture platforms†

Sandra Ramos-Díez,*[a] Garazi Larrañaga-Jaurrieta,*[a,b] Leire Iturriaga,[a] Ander Abarrategi [b,c] and Sandra Camarero-Espinosa [a,c]

Digital light processing (DLP) printing offers the possibility of fabricating complex objects in a fast and reproducible manner. A main requirement for DLP printing is the use of inks with low viscosities that can flow under the printing platform in a short period of time. Its exploitation in tissue engineering applications has been centered on the use of hydrogel forming materials diluted in aqueous solutions or the use of polyesters in combination with diluents and heating platforms that aid in the reduction of their viscosity. The use of diluents, however, modifies the mechanical properties and reduces the shape fidelity of the printed objects and, the use of heating platforms results in vats with heterogeneous temperatures and ink viscosities. Here, we report on the synthesis of a library of methacrylated low molecular weight (<3000 g mol^{-1}) homopolymers ((P(D,L)LA and PCL) and copolymers (P((D,L)LA-*co*-CL)) of 2- and 3-arms based on (D,L)-lactide and ε-caprolactone. The resulting inks possessed low viscosity that made them printable in the absence of diluents and heating elements. DLP printing of cubical and cylindrical patterns resulted in objects with a higher shape fidelity than their counterparts fabricated using diluents and with printed features on the order of 300 μm. The printed materials were biocompatible and supported the growth of human mesenchymal stem cells (hMSCs). Moreover, the variations in the composition resulted in polymers that enabled the attachment of hMSCs to different extents, leading to the formation of well-adhered cell monolayers or loosely adhered cell aggregates.

Received 7th April 2023,
Accepted 29th June 2023

DOI: 10.1039/d3bm00581j

rsc.li/biomaterials-science

1. Introduction

Additive manufacturing, in particular three-dimensional (3D) printing, has attracted exceptional interest in the last decade due to its undeniable advantages, such as the easy and fast fabrication of objects with complex structures at reduced costs and has found application in numerous and varying fields including dental applications, prototyping, tissue engineering and tissue regeneration.[1–3] Furthermore, the wide scope of different available 3D printing technologies enables the use of materials with different characteristics as inks derived from metals[4] to hydrogels,[2] passing through ceramics and polymers.[5] Light based 3D printing technologies such as 2-photon polymerization (2PP), digital light processing (DLP) and stereolithography (SLA) offer the possibility of printing most complex structures commonly required in the field of tissue regeneration and great advances have been made in the last few years, including volumetric 3D bioprinting.[6–8] The main difference between them is that the last two, DLP and volumetric 3D bioprinting, use a light projector to create 3D objects instead of a laser, reducing significantly the printing time. While volumetric 3D bioprinting permits the fabrication of objects in extremely short times, it has a very restricted window of materials that can be used, as they have to be solid or gel-like during the fabrication process.

The DLP printing technique has aroused great interest since it has proven to be a fast (from 25 to 1000 mm min^{-1}) and reproducible manufacturing method with high efficiency and theoretical resolutions of a few microns (~10 μm).[9–11] Nevertheless, these parameters vary in function of the experimental set-up, specifically in function of the viscoelastic properties of the selected resin, the intensity of the light source, the photosensitivity of the ink and the overall concentration and the nature of cross-linkable groups contained in the ink.[3]

In this regard, the choice of inks used for DLP printing is crucial; it will not only determine the spatial resolution, surface chemistry or mechanical properties, but will also define the biocompatibility and degradability of the final

[a]*BioSmarTE Lab, POLYMAT, University of Basque Country UPV / EHU, Donostia / San Sebastián 20018, Gipuzkoa, Spain. E-mail: sandra.camarero@ehu.eus*
[b]*Regenerative Medicine Lab, CICbiomaGUNE, Donostia / San Sebastián 20014, Gipuzkoa, Spain*
[c]*Ikerbasque, Basque Foundation for Science, Euskadi Pl., 5, 48009, Bilbao, Spain*
† Electronic supplementary information (ESI) available. See DOI: https://doi.org/10.1039/d3bm00581j

model. Most of the studies using DLP printing for tissue engineering constructs have been focused on the use of hydrogel forming materials such as those based on polyethylene glycol (PEG), gelatin, hyaluronic acid or silk.[8–10,12] Polyester-based polymers such as poly(lactide) (PLA),[13,14] poly(ε-caprolactone) (PCL)[15–17] and poly(trimethylene carbonate) (PTMC)[18] are commonly used in tissue engineered scaffolds including those fabricated by DLP, as they can be synthesised by ring-opening polymerization (ROP) allowing the control of the polymer structure and chain length.[19] One of the main requirements for good printability is the low viscosity (<10 Pa s) of the resin and a Newtonian response to shear,[3,19] as it will determine the ability of the material to flow under the crosslinked layer in between the sliced projections. Polymers with a high molecular weight or semicrystalline structures, like the aforementioned polyesters, generally result in viscous (or even solid) resins which are incompatible with DLP printing. Thus, they are combined with reactive or non-reactive diluents and heating elements to lower their viscosity into the printable regime. Reactive diluents such as 2-(2-ethoxyethoxy)ethyl acrylate (EOEOEA) or *N*-vinyl-2-pyrrolidone (NVP) are incorporated in the bulk of the printed objects compromising their mechanical properties and altering the preselected chemistry of the inks;[14,18] non-reactive diluents such as ethylene lactate or dioxane are washed away after printing, compromising the structural stability of the object[17,20] and, heating stages require the design of home-made set-ups with vague control of the applied temperatures and size limitations in the printed object derived from the heterogeneous temperatures in larger vats.[21]

Melchels *et al.*[20] synthesised star-shaped methacrylated P(D,L)LA inks with 2–, 3- and 6-arms and DLP printed them using ethylene lactate as non-reactive diluent. All the reported mixtures had viscosities below 10 Pa s. They selected those with the highest diluent concentration (19 wt%) for printing, yielding inks with viscosities of approximately 1 Pa s. While the resulting materials after DLP printing proved biocompatible, the use of a non-reactive diluent led to a shrinkage of 10% (in all directions) when complex gyroid structures were created. Similarly, Paunović *et al.*[16] synthesised 4-arm methacrylated P((D,L)lactide-*co*-caprolactone) (P((D,L)LA-*co*-CL)-MA low molecular weight (<9000 g mol^{-1}) copolymers by ROP. The neat polymer showed a viscosity of over 40 Pa s when heated at 60 °C, which decreased to below 5 Pa s when mixed with 7.5 wt% NVP reactive diluent. The printed objects possessed structural features on the mm scale, probably due to the still high viscosity of the inks that yield low-resolution objects. The mechanical properties of the printed polymer with NVP were of 4 MPa, which appears to be very low for a P((D,L)LA-*co*-CL copolymer, probably due to the incorporation of the reactive diluent in the bulk.

Kuhnt *et al.*[18] reported on the synthesis of DLP inks based on poly(caprolactone-*co*-trimethylenecarbonate) urethane acrylates and used 30 wt% EOEOEA as the reactive diluent and a heating platform to further decrease the viscosity of some of their ink compositions.[21] They neatly showed the capability of tuning the mechanical properties of their inks from 0.2–5.4 MPa by varying the ratio of caprolactone to trimethylenecarbonate, which also affected the morphology of adhered cells. Nevertheless, the mechanical properties were lower than those expected for films fabricated from these types of polyester urethanes, which could be explained by the large amount of reactive diluent required for DLP printing. The same group recently reported on the scaled-up synthesis of P((D,L)LA-*co*-CL)-MA inks for DLP printing. In this work, they studied resins with molecular weights ranging from 1000 to 10 000 g mol^{-1}.[22] Despite reporting on the inks being liquid, a 30 wt% EOEOEA reactive diluent was added to the polymer and a heating stage was used for DLP processing.

Due to the lack of biocompatible resins with a suitable viscosity that can be DLP printed without the use of diluents or heating stages, in this work, we strove to develop liquid biocompatible inks based on (D,L)-lactide and ε-caprolactone monomers. We hypothesised that low molecular polymers could result in liquid inks. We created a library of homopolymers and copolymers with 2- and 3-arms and investigated the effect of the different monomers and the steric hindrance of the chains on the viscosity of the resulting ink.

2. Experimental section

2.1. Materials

Triethylene glycol (TEG), tin(II) 2-ethylhexanoate ($Sn(Oct)_2$), methacrylic anhydride (MMA), sodium bicarbonate ($NaHCO_3$), diphenyl(2,4,6-trimethylbenzoyl)phosphine oxide (TPO), sodium chloride (NaCl), and triethanolamine (TEA) were purchased from Sigma-Aldrich. (D,L)-lactide and hydroquinone were obtained from Acros. Dichloromethane (CH_2Cl_2) anhydrous and methanol were purchased from Scharlau. ε-caprolactone, dimethyl sulfoxide (DMSO), and 2-ethyl-2-(hydroxymethyl)-1,3-propanediol (TMP) were supplied by Alfa-Aesar. Deuterated chloroform ($CDCl_3$) was obtained from VWR Chemicals.

2.2. Synthesis of polymers and methacrylation procedure

All polymers were synthesised by ring-opening polymerization. To synthesise **2-** and **3-arm-P(D,L)LA**, 25.85 g (0.18 mol) of (D,L)-lactide was added to a round-bottom flask and heated to 130 °C under vigorous stirring until molten, under a N_2 atmosphere. Then, 3 mL of TEG (0.022 mol) or 2 g of TMP (0.015 mol) was added for 2- and 3-arm polymers, respectively. Yields of 64.9% and 71.3% were obtained respectively. For the synthesis of **2-** and **3-arm-PCL**, 19.0 mL of ε-caprolactone (0.18 mol) was added to a round-bottom flask under vigorous stirring and a N_2 atmosphere. Then, 3 mL of TEG (0.022 mol) or 2 g of TMP (0.015 mol) was added. Yields of 78.0% and 83.5% were obtained respectively. For the synthesis of **2-arm-P((D,L)LA-*co*-CL)**, 5.43 g of (D,L)-lactide (0.037 mol) was melted in a round-bottom flask at 130 °C under a N_2 atmosphere. Then, 15.0 mL of ε-caprolactone (0.14 mol) and 3 mL of TEG (0.022 mol) were added to the flask. A yield of 98.2% was obtained. For the synthesis of **3-arm-P((D,L)LA-*co*-CL)**, 5.36 g of

(D,L)-lactide (0.037 mol) were melted in a round-bottom flask at 130 °C together with 2 g of TMP (0.015 mol). Later, 14.8 mL of ε-caprolactone (0.14 mol) was incorporated. A yield of 98.7% was obtained.

To all reactions, 0.28 mL of 1 : 10 (vol : vol) $Sn(Oct)_2$: toluene catalyser solution (0.088 mmol) was subsequently added. The reactions were carried out for 24 hours at 130 °C. After the reaction, the product was washed three times by precipitation in methanol and dried under vacuum. For the methacrylation step, 5 g of purified polymer was dissolved in 5 mL of anhydrous CH_2Cl_2 by gentle ultrasonication for 10 minutes. The solution was then poured over 5 mg of hydroquinone (0.045 mmol) in a round-bottom flask in the dark and under a N_2 atmosphere. Afterwards, 3 : 3 or 4 : 4 ratio (mol : mol) of TEA : MAA per mol of oligomer was added to 2- and 3-arm polymers, respectively. The reaction was left to proceed for 48 hours at room temperature. The product was recovered by phase separation with both saturated $NaHCO_3$ and brine solutions, consecutively. The organic extract was firstly concentrated in a rotary evaporator at 60 °C, precipitated three times in methanol at 4 °C and dried under vacuum. Yields between 70% and 90% were obtained after the purification step in all the methacrylated polymers.

2.3. Characterization of polymers

2.3.1. ^{1}H-NMR spectroscopy of synthesised polymer intermediates and methacrylated polymers. Samples for NMR analysis were prepared in $CDCl_3$ and analysed on a Bruker NMR 500 MHz Advance spectrometer (Bruker BioSpin, Rheinstetten, Germany). The efficiency of each reaction and the degree of methacrylation (DoM) of the resulting polymers were determined by means of ^{1}H-NMR spectroscopy as the ratio between the peaks at 1.99 ppm and at 3.65 ppm, corresponding to the protons of CH_3 of MA and CH_2 of TEG in 2-arm polymers, respectively. In the case of 3-arm polymers, the selected ratio was between the peaks at 1.99 ppm and 0.91 ppm, corresponding to the protons of CH_3 of MA and CH_3 of TMP, respectively. Details of H^1-NMR shifts are provided in the ESI file.†

2.3.2. Differential scanning calorimetry (DSC). A DSC3+ (Mettler Toledo) equipment was used for the thermal characterization of all the polymers. Samples of 4–10 mg were analysed under N_2 atmosphere (50 ml min^{-1}) in a thermal cycle consisting of a first heating from −80 °C to 200 °C at a heating rate of 20 °C min^{-1}, followed by a cooling cycle from 200 °C to −80 °C at 10 °C min^{-1} and a last heating step from −80 °C to 200 °C with a heating rate of 20 °C min^{-1}. The reported thermal transitions were obtained during the second heating cycle.

2.3.3. Gel permeation chromatography (GPC). The molecular weights and distributions were measured for each material in tetrahydrofuran (THF) as the solvent and at 1 ml min^{-1} flow rate. The GPC group consisted of a refractive index detector model 2414 (Waters), LC-20AD pump (Shimadzu), 717 plus autoinjector (Waters) and low molecular weight columns: Starygel Guard Column, Styragel HR4, Styragel HR2 and Styragel HR1 (Waters) calibrated in the range of 162–436 200 g ml^{-1}. The temperature of the columns was 35 °C.

2.3.4. Rheological and photorheological characterization. Rheological measurements were conducted in an AR-G2 photorheometer (TA instruments) with a disposable aluminium parallel plate of 20 mm diameter and a UV module (365 nm). All the resins were prepared by adding 5% (w/w) of diphenyl(2,4,6-trimethylbenzoyl)phosphine oxide (TPO) photoinitiator and placed in the oven at 25 °C until running the experiment. Prior to measuring the photorheological properties of the methacrylated polymers, an oscillation amplitude test was performed from 1% to 1000% strain to find the linear region of deformation of the resins and the viscosity at 25 °C that would determine the printability of the material. Subsequently, photorheology was used to analyse both the elastic and viscoelastic behaviour of the materials during irradiation using a 200 mW cm^{-2} intensity UV lamp. The strain was determined specifically for each resin depending on its linear region of deformation from the initial rheological measurements. The gap distance between the parallel plates and the UV module was set to 220 μm and the frequency 1 Hz for all measurements. The measurements were run for 150 seconds, with an irradiation time of 60 s, after settling for 30 s.

2.3.5. Mechanical characterization. Tensile tests were conducted on a TA·HD Plus texture analyzer (Stable Micro Systems, UK) equipped with a 30 kg load cell at 0.01 mm s^{-1} strain and with a preload of 0.2 N. Samples of 2- and 3-arm copolymers and homopolymers were 3D printed or casted and UV cross-linked to fit 5 × 20 mm samples. Young's moduli were calculated from stress–strain curves between 0.2 and 1% strain.

2.4. Cell adhesion and biocompatibility studies

To study cell biocompatibility and adhesion, films of 7 × 7 × 0.4 mm were prepared using the DLP Titan 2 HR (KUDO 3D) printer for both P((D,L)LA-*co*-CL)-MA copolymers of 2- and 3-arms. Homopolymer films were prepared by adding 500 mg of each sample between two coverslips and curing them by UV exposure with a lamp operating at 405 nm wavelength and 48 W power (post-curing LED Lamp KUDO 3D). All samples were submerged in 1 : 2 (vol : vol) isopropanol : acetone solution for 10 minutes to remove the non-cured ink. Afterwards, the films were sterilised in ethanol at 70% for 15 minutes. Samples were then rinsed three times with PBS and placed in non-treated 24-well plates containing complete culture media 30 min before use.

2.4.1. Cell culture. Human bone marrow mesenchymal stem cells (hMSC) were purchased from StemCell™ Technologies (Donor 2111410009) in passage 0. hMSCs were expanded in a monolayer culture at a density of 3.3×10^3 cells per cm^2 and in α-MEM supplemented with 10% (v/v) fetal bovine serum (FBS) at 37 °C with 5% of CO_2 until 80% confluence. The culture media was changed every 2–3 days. Phosphate buffer saline (PBS) was used to wash adherent cells before their detachment with 0.25% Trypsin/EDTA solution (Gibco™). hMSCs resuspended in α-MEM supplemented with

10% (v/v) FBS were seeded on the sterilized films at a density of 60 000 cells per cm^2.

2.4.2. DNA assay. The total DNA content was measured with a CyQuant™ cell proliferation assay (Invitrogen), following manufacturer's instructions and assuming 6.6×10^{-6} μg of DNA per cell to estimate cell numbers. hMSCs were cultured on the prepared films for 24 hours and washed with DPBS three times to remove the media. Samples were first freeze–thawed 3 times and digested using 1 mg ml^{-1} Proteinase K (Fisher BioReagents™) in Tris/EDTA buffer at 56 °C overnight. Serial dilutions of the DNA standard from the CyQuant™ kit ranging from 2 μm ml^{-1} to 0 μm ml^{-1} were prepared for the standard curve. Afterwards, lysis buffer containing RNase diluted 1 : 500 was added to each sample in a 1 : 1 ratio, mixed and incubated at RT for 1 hour to degrade the cellular RNA. In parallel, the GR-dye stock solution was diluted 200-fold into the lysis buffer. Finally, 100 μl of each sample was transferred to a well of a black bottom microplate in triplicate. After adding 100 μl of the GR-dye solution and incubating for 15 minutes at RT, fluorescence was measured at 480 nm excitation and 520 nm emission.

2.4.3. Cell adhesion and viability. The cell adhesion to the films was evaluated after 24 hours of culture by fluorescence microscopy. To that end, films were washed twice with DPBS and the cells were fixed by incubation in a solution of 4% paraformaldehyde (PFA) for 15 minutes. The cells were then permeabilized in a solution of 0.1% Triton™ X-100 (Fisher BioReagents) in PBS for 15 minutes and then washed again twice with PBS. Cells were stained with Phalloidin Alexa Fluor 488 (1 : 100) in PBS for 1 h, rinsed twice with PBS and stained for 5 min with Hoechst 33342 (1 : 500) (Invitrogen, Thermo Scientific).

The cell viability was evaluated by LIVE/DEAD™ viability/cytotoxicity kit for mammalian cells (Invitrogen) following manufacturer's instructions. Briefly, 24 h after cell seeding in the films the culture media was removed and the films were washed 2 times with DPBS. Afterwards, 1 ml of 6 μM ethidium homodimer and 1 μl of 1 mM Calcein were combined and 300 μL of the solution were used to cover each polymer film. The cells were incubated for 45 min protected from light and the staining solution was replaced with DPBS. The samples were visualized immediately under a fluorescence microscope at 518 nm and 540 nm for live and dead cells, respectively.

2.4.4. Fluorescence microscopy. Fluorescence images of adhesion were recorded using an Axio Observer (Zeiss) cell observer fluorescence microscope equipped with a metal halide arc lamp HXP-120 (Zeiss) and an AxiocamMRR3 (Zeiss) camera. Fluorescence images of live/dead experiments were recorded on a Nikon Eclipse-Ti2-E equipped with an LED based Lumencor Spectra II Illuminator and a large field Photometrics Iris 15 sCMOS camera.

2.5 DLP printing of structures with micro-topographical features

The models were designed using Solid Edge (Siemens) CAD software and exported as STL file for subsequent treatment with Kudo 3D slicing software. PNG images were created for each slice of 15 μm height composed of 32 bits per pixel. Models of cubes and cylinders had a base of 7 × 7 mm and 0.35 mm in height. The surface pattern was created as a matrix of 8 × 8 elements of 0.3 × 0.3 × 0.3 mm cubes or 0.3 ∅ × 0.3 mm pillars. In all cases, the first layer was irradiated for 50 seconds to ensure the attachment of the model to the platform. The rest of the layers of the base were irradiated for 5 seconds and the layers corresponding to the topography for 8 seconds.

2.5.1. Scanning electron microscopy and printing error. Visualization of the printed micro-topographies was accomplished by scanning electron microscopy (SEM) using a TM3030Plus SEM (Hitachi High-Technologies) apparatus at different magnifications operating at 15 keV. The surface of the samples was previously gold-coated using an SC7620 mini sputter coater/glow discharge system (Quorum).

The printing error of the models was measured from the SEM images, taking into account the width of the cubes or the diameter of the pillars and the height of the topography, following the equation:

$$\varepsilon_x = \frac{X_r - X_t}{X_r} \times 100$$

where ε_x is the error in the width (ε_w), in the diameter ($\varepsilon_\varnothing$) or in the height (ε_h). X_r and X_t are the real and theoretical dimensions, respectively.

2.6. Statistical analysis

The statistical analysis was performed using GraphPad Prism 8 (GraphPad Software, San Diego, CA, USA). One-way and two-way analyses of variance (ANOVA) were carried out for complex viscosity, storage modulus G' values, Young's modulus, elongation at break, maximum stress and cell viability assays to calculate the significance and including a *post-hoc* Tukey's multiple comparison test. All the results are expressed as mean values ± standard deviation.

3. Results and discussion

3.1. Synthesis and characterization of low molecular weight PCL- and P(D,L)LA-based polymers and copolymer inks

Polylactide (P(D,L)LA) and polycaprolactone (PCL) are among the most commonly used polyesters for the biofabrication and additive manufacturing of tissue engineering and regeneration scaffolds due to their biocompatibility, their ease to be processed and shaped into complicated structures, their structural stability and their relatively high mechanical properties. However, their application in DLP printing is restricted due to their high viscosity at room temperature, requiring the use of (reactive) diluents or heating platforms that make the fabrication process difficult and limit the resolution of the obtained structures.[13,16,18,21] We hypothesised, that low molecular weight P(D,L)LA and PCL homopolymers and copolymers thereof, would result in materials of lower viscosity and that

after methacrylation, could be exploited in the DLP biofabrication process without the use of heating platforms and/or diluents. Hence, low molecular weight (<3000 g mol^{-1}) resins were synthesised from (D,L)-lactide (LA) and ε-caprolactone (CL) monomers. Homopolymers and copolymers were synthesized as 2- and 3-arm polymers to obtain, after methacrylation, a high density of photoreactive motifs that could speed up the printing process and yield materials with higher cross-linking densities and printing resolutions. 2-arm and 3-arm polymers and copolymers were synthesised by ring-opening polymerization using triethylene glycol (TEG) or 2-ethyl-2-(hydroxymethyl)-1,3-propanediol (TMP) at 8 : 1 and 12 : 1 monomer to initiator ratios, respectively (Scheme 1A). P((D,L)LA-*co*-CL) copolymers were synthesized using the same monomer to initiator ratio with a 1 : 3.76 LA : CL ratio and with the addition of stannous octanoate as catalyst (Table 1). H^1-NMR spectroscopy was used to evaluate the successful polymerization of the polymers (Fig. S1†). For 2-arm polymers, chemical shifts at δ = 3.65 ppm, corresponding to CH_2 adjacent to the terminal monomer-bound TEG, were observed as a triplet, while terminal –OH groups corresponding to free TEG were not detected (expected as a triplet at δ = 3.56 ppm). For 3-arm polymers, monomer-bound TMP showed a singlet at δ = 4.02 ppm as opposed to the singlet at δ = 3.39 ppm of TMP-free terminal –OH groups. Moreover, in the case of PCL homopolymers and copolymers, a peak at δ = 2.23 ppm corresponding to the CH_2 nearest to the formed ester bond was detected (labelled in grey in Fig. S1†). The ratio of LA : CL in the copolymers was calculated using the integrals of CH protons appearing at δ = 3.51 ppm for P(D,L)LA and CH_2 nearest to carboxylic proton, appearing at δ = 2.23 ppm for PCL (shown respectively as black and grey dots in Fig. 2). This ratio was slightly lower than the

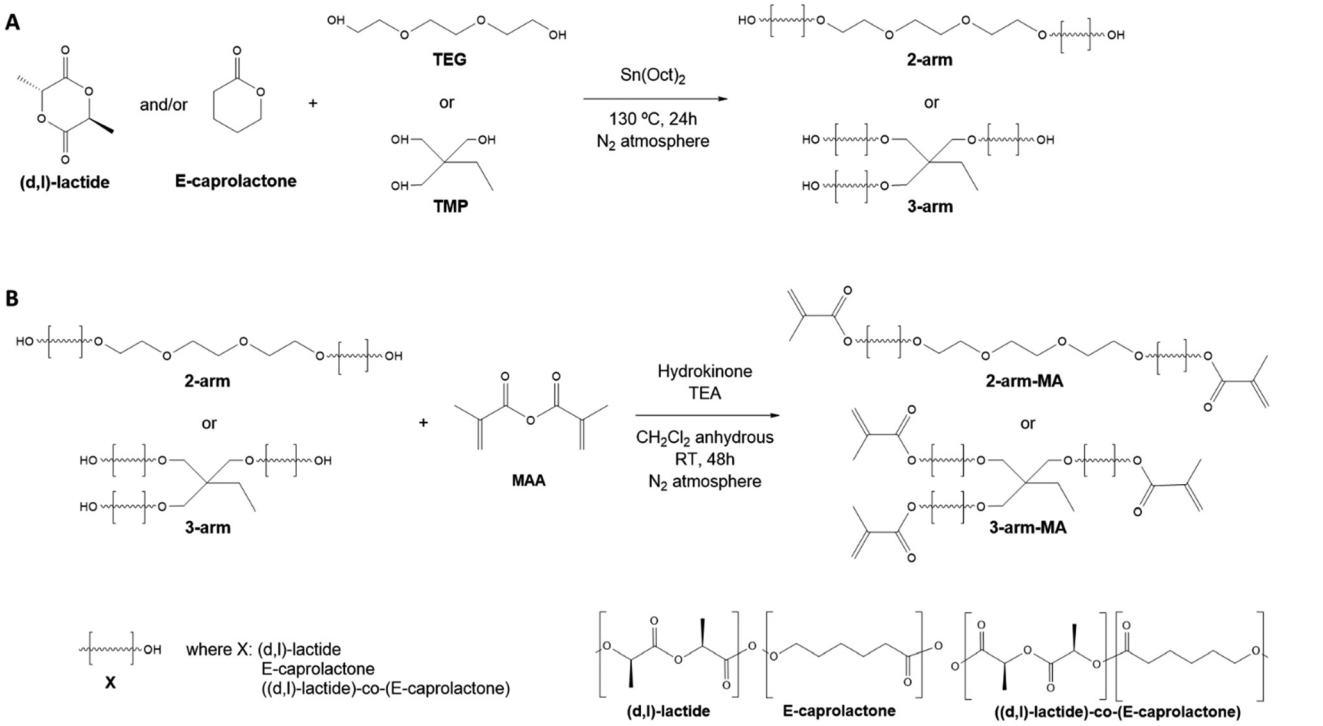

Scheme 1 (A) Ring-opening polymerization reaction to synthesize 2- and 3-arm homopolymers and copolymers of lactide and caprolactone using TEG or TMP as co-initiator, respectively, and Sn(Oct)$_2$ as catalyst. (B) Methacrylation reaction that introduces photocross-linkable terminal groups on 2- (top) and 3-arm (bottom) homopolymers and copolymers employing hydroquinone as catalyst.

Table 1 Synthetic properties of methacrylated polymers measured by ^{1}H-NMR and GPC

Polymer	Theor·LA : CL ratio (mol : mol)	Product LA : CL ratio (mol : mol)	*D* of methacrylation (%)	Theor. M_w (g mol^{-1})	M_w (g mol^{-1})	M_n (g mol^{-1})	M_w/M_n	Appearance
2-arm-P(D,L)LA	1 : 0	1 : 0	88	1303.18	1264	1572	1.24	Very viscous liquid
2-arm-PCL	0 : 1	0 : 1	61	1063.33	1670	2310	1.38	Waxy solid
2-arm-P((D,L)LA-*co*-CL)	1 : 3.76	1 : 2.93	98	1123.29	1559	2197	1.40	Viscous liquid
3-arm-P(D,L)LA	1 : 0	1 : 0	100	1863.69	2093	2559	1.22	Very viscous liquid
3-arm-PCL	0 : 1	0 : 1	96	1503.9	2187	2606	1.19	Waxy solid
3-arm-P((D,L)LA-*co*-CL)	1 : 3.76	1 : 3.12	99	1593.85	2188	2918	1.33	Viscous liquid

feed ratio and we hypothesised that LA has a higher reactivity than CL monomers.

Gel permeation chromatography revealed that all polymers had a low molecular weight ranging from ≈1200 to 2200 g mol-1 (Table 1 and Fig. S2†), which varied slightly with respect to the calculated theoretical value. This low molecular weight resulted in polymers with lower viscosities as compared to the traditional solid powders obtained for high molecular weight PLA, PCL and copolymers thereof. Indeed, 2- and 3-arm P(D,L)LA appeared as very viscous liquids, while 2- and 3-arm PCL resulted in waxy solids and, the 2- and 3-arm P((D,L)LA-*co*-CL) copolymers in viscous liquids.

Analysis of the thermal properties of the synthesised inks *via* dynamic scanning calorimetry (DSC, Fig. 1) showed, as expected, that 2- and 3-arm P(D,L)LA resulted in amorphous polymers with no melting transitions (T_m) and with glass transition temperatures (T_g) of −8 °C and 17 °C, respectively. 2- and 3-arm PCL homopolymers presented T_g at −65 °C and −58 °C, respectively. PCL homopolymers showed in both cases two distinct T_m of 32 °C and 42 °C for the 2-arm-PCL and 15 °C and 28 °C for the 3-arm-PCL. The double melting peaks observed in PCL polymers are relatively common in polyesters. We hypothesised that these two peaks correspond to the reorganization of the crystal structures during the heating process whereas the thinner lamellar structures formed during the cooling process melt, recrystallizing into thicker lamellae that melt at a higher temperature. Another possibility would be the formation of extended-chain and folded-chain crystal structures, due to the low molecular weight polymers, that results again in lamellae of different thicknesses. This behaviour is not observed during the cooling process, where a single crystallization peak is detected at 16 °C and −8 °C for the 2- and 3-arm homopolymers respectively, as this one is generally dominated by the density of active nucleating sites. 2- and 3-Arm P((D,L)LA-*co*-CL) copolymers showed a thermal response characteristic of amorphous polymers with T_g at −55 °C and −48 °C, respectively and no associated melting transitions, further confirming the formation of copolymers.

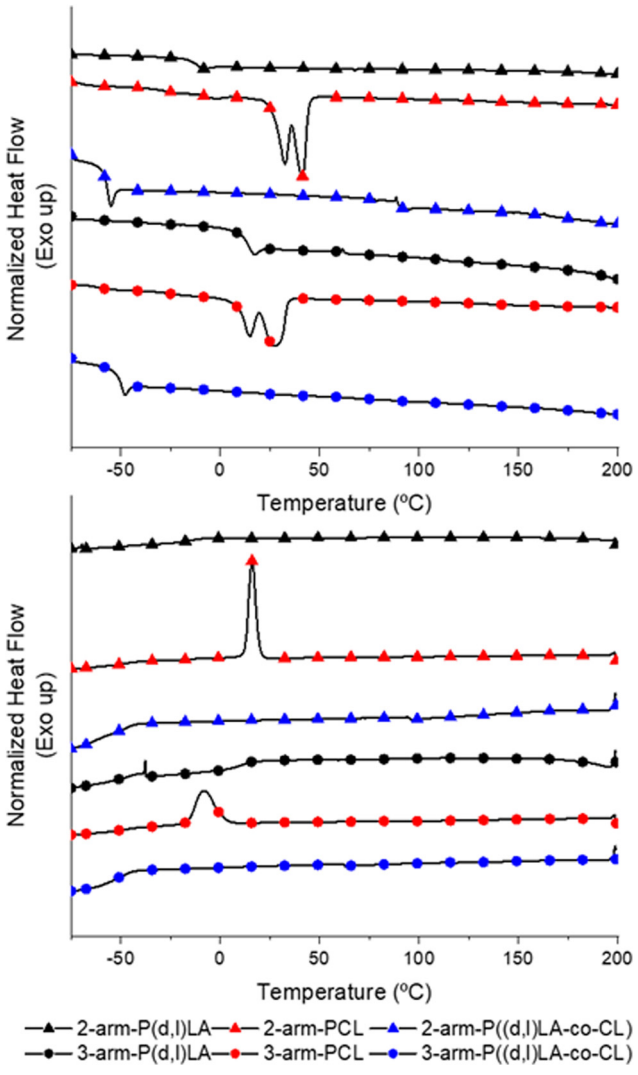

Fig. 1 DSC thermograms of second heating scans (top) and cooling scans (bottom) of synthetized 2-arm (▲) and 3-arm (●) P(D,L)LA, 2-arm (▲) and 3-arm (●) PCL and 2-arm (▲) and 3-arm (●) P((D,L)LA-co-CL) polymers.

Having characterized the homopolymers and copolymers synthesized, we proceeded with the methacrylation of the terminal –OH groups (Scheme 1B). For that, the dry polymers were reacted with methacrylic anhydride in the presence of triethanolamine and hydroquinone. The methacrylated polymers were then analysed by H^1-NMR (Fig. 2), where the characteristic doublets associated to the CH_2═C bond of the methacrylic group were detected in all compounds. These protons associated to the methacrylic groups in methacrylated P(D,L)LA and PCL (P((D,L)LA-MA and PCL-MA) presented slightly different shifts at δ = 6.23 ppm and δ = 5.69 ppm, and δ = 6.15 ppm and δ = 5.60 ppm, respectively. These peaks were also detected in the methacrylated copolymers (P((D,L)LA-*co*-CL)-MA), indicating that the arms had different compositions and terminal repeating units. We hypothesized that these mild differences are due to the charge deshielding that carboxylic groups from PLA repeating units induce into methacrylic protons, which results in an increase in their chemical shifts. The degree of methacrylation of 2- and 3-arm methacrylated polymers was calculated from the ratio of the mentioned peaks and both CH_2 signals from TEG at δ = 3.65 ppm and δ = 4.33 ppm, or CH_3 signal from TMP at δ = 0.91 ppm, ranging from 61 to 100% (Table 1).

3.2 Printability and viscoelastic properties of DLP resins

To evaluate the printability of the synthesized resins *via* DLP or lithographic techniques, the viscoelastic properties were measured by rheological analysis (Fig. 3). Too viscous resins require the use of diluents that reduce the viscosity and enable the fast penetration of the ink underneath the printing platform and object when the platform is raised between the printed layers. Moreover, inks presenting a non-Newtonian response to shear–stresses could change their viscosity upon displacement of the printing platform, reducing their capa-

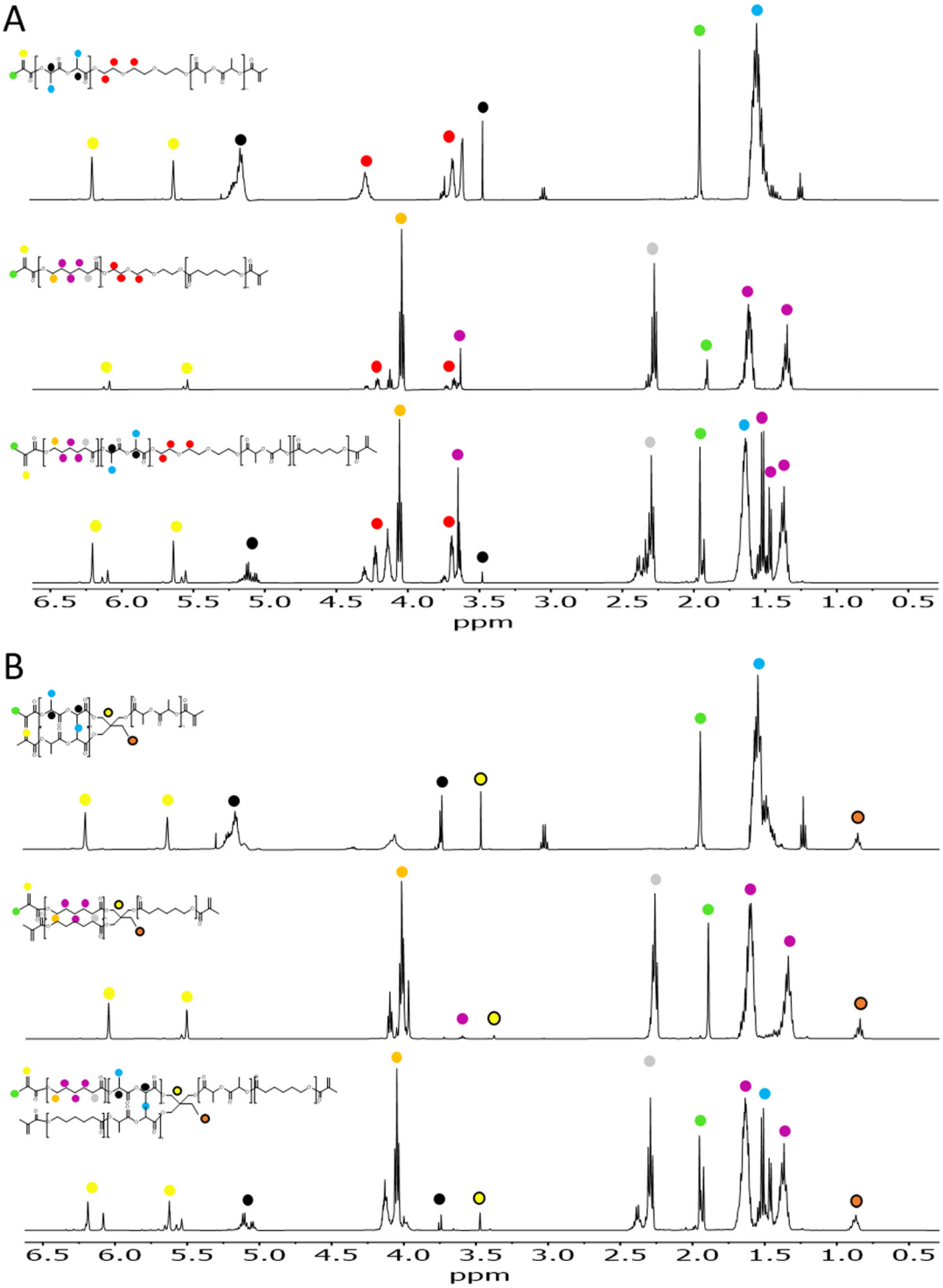

Fig. 2 ^{1}H-NMR spectrum of 2- (A) and 3-arm (B) methacrylated polymers in $CDCl_3$. (top) P(D,L)LA-MA, (middle) PCL-MA and (bottom) P((D,L)LA-*co*-CL)-MA. The identified proton signals are associated to the molecular structure with coloured circles.

bility to flow and cover the printing vat and the speed at which the platform can be displaced. All resins presented a Newtonian response, as evidence by the constant complex viscosity recorded for the tested oscillation rates and the linear increase in oscillation stress with the oscillation rate (Fig. 3A). Complex viscosity values ranged from 1–70 Pa s, depending on the polymer composition and the number of arms. The complex viscosity appeared to decrease for all polymers and copolymers with an increasing number of arms (although not statistically significant for all), probably as a result of the higher electrostatic hindrance between adjacent arms in a same polymer chain (Fig. 3A). PCL-based polymers presented

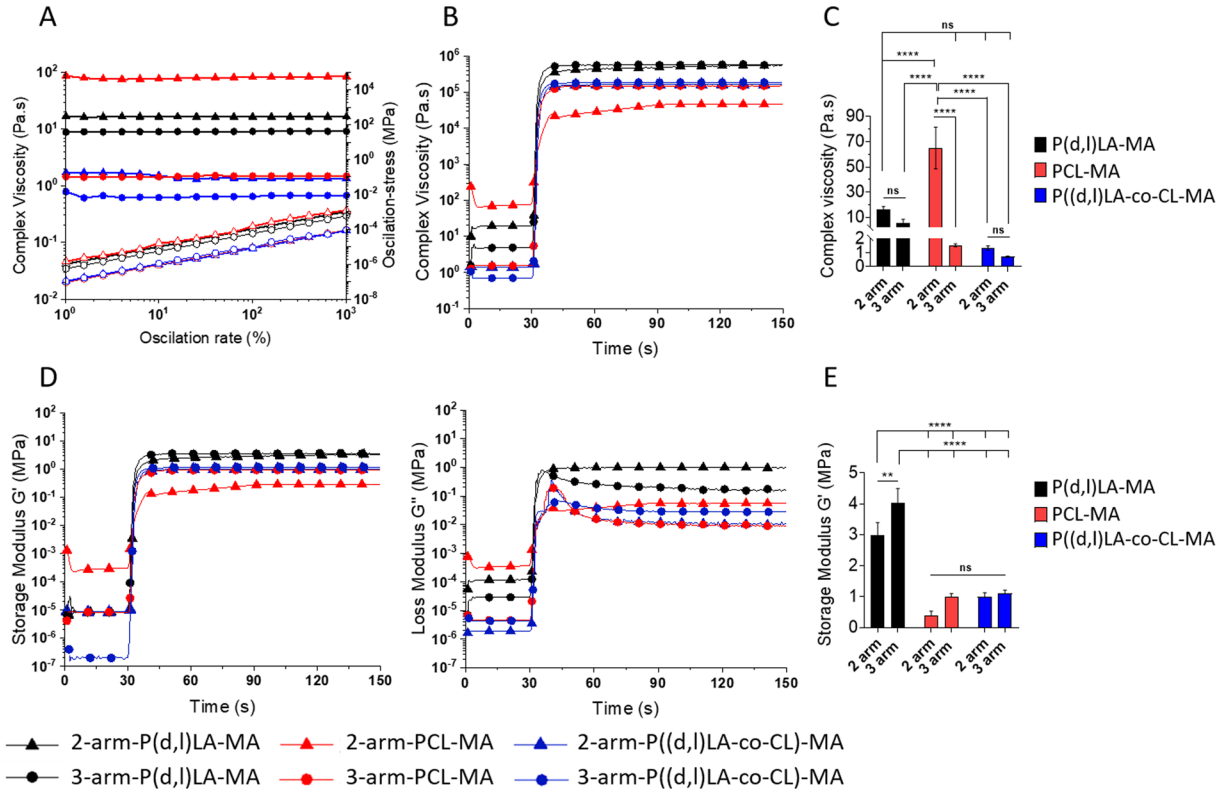

Fig. 3 Viscosity measurements of the resins as a function of the oscillation rate (strain sweep) (A), from 1 to 1000% of deformation, and (B) variation of the complex viscosity as a function of time and upon irradiation with UV light. (C) Statistical analysis of the average complex viscosity of the inks before photocross-linking. Statistical significance was calculated from two-way ANOVA with Tukey's multiple comparison test. For complex viscosity: interaction $F(2,12) = 35.28$, $p < 0.0001$; arm number $F(1,12) = 58.04$, $p < 0.0001$; material type $F(2,12) = 33.90$, $p < 0.0001$. Adjusted p-values: $p < 0.1$ (ns), $p < 0.0322$(*), $p < 0.0021$ (**), $p < 0.0002$ (***) and <0.0001 (****). (D) Elastic (left, Storage Modulus G') and viscoelastic (right, Loss Modulus G'') response of the inks upon irradiation with 200 mW cm^{-2} UV light module (365 nm) for 60 seconds after a settling time of 30 seconds. (E) Storage Modulus G' of crosslinked materials at plateau. Statistical significance was calculated from two-way ANOVA with Tukey's multiple comparison test. For complex viscosity: interaction $F(2,12) = 4.098$, $p = 0.0440$; arm number $F(1,12) = 20.04$, $p = 0.0008$; material type $F(2,12) = 183.2$, $p < 0.0001$. Adjusted p-values: $p < 0.1$ (ns), $p < 0.0322$ (*), $p < 0.0021$ (**), $p < 0.0002$ (***) and <0.0001 (****).

the highest viscosity with values of 65 ± 16 Pa s for the 2-arm-PCL-MA and decreasing to 1.5 ± 0.1 Pa s when presenting 3-arms. PLA-based inks presented a viscosity of 16 ± 2 and 5 ± 3 Pa s for the 2-arm and 3-arm-PLA-MA, respectively. Copolymers of P((D,L)LA-*co*-CL)-MA showed the lowest viscosities with values of 1.4 ± 0.2 and 0.72 ± 0.05 Pa s for the 2- and 3-arm versions. The optimal viscosity of inks for DLP and SLA printing has been set in the range of 0.1–10 Pa s.[3] Thus, 2-arm-PCL-MA and 2-arm-P(D,L)LA-MA polymers appeared to be too viscous to be printed without the incorporation of diluents or the use of heating sources (Fig. 3C).

Oscillatory measurements were carried out during UV exposure to evaluate the kinetics of the curing process. Upon irradiation with UV light, the viscosity of all the materials increased rapidly and exponentially, reaching a plateau as soon as 1–2 s after the irradiation was started, demonstrating the fast crosslinking speed of the resins (Fig. 3B and Fig. S3†). The complex viscosity of the photocross-linked materials was the highest for 2- and 3-arm-P(D,L)LA-MA polymers, followed by 2- and 3-arm-PCL and P((D,L)LA-*co*-CL) copolymers (Fig. 3C). In all cases, 3-arm polymers displayed a higher complex viscosity after cross-linking than their 2-arm counterparts, as a result of the higher cross-linking density. P(D,L)LA-MA, PCL-MA and P((D,L)LA-*co*-CL)-MA films prepared from 2-arm and 3-arm polymers were attributed for a complex viscosity of 502 ± 36 and 572 ± 9, 42 ± 6and 150 ± 0.9 and, 162 ± 1 and 185 ± 1 kPa s, respectively.

To evaluate the viscoelastic properties of the liquid resins and the cross-linked materials, the storage (G') and loss moduli (G'') of the resins were measured before and after UV irradiation during oscillatory photorheological experiments (Fig. 3D and E). G' and G'' represent the elastic and viscous components of a viscoelastic material, respectively. Readily upon UV irradiation both, G' and G'', increased over five orders of magnitude in all inks demonstrating the cross-linking of the chains. 2-arm-PCL-MA, which was initially a waxy solid, suffered an increase of G' and G'' of only 3 orders of magnitude, yet, indicating the cross-linking of the resin. 2- and 3-arm P((D,L)LA-MA, 2-arm PCL-MA and P((L,D)LA-*co*-CL)-MA inks displayed a G' that was lower than G'' at the beginning of the measurement and before UV irradiation, which increased upon UV irradiation crossing at the gelling point, to give rise

to solid resins with an elastomeric response (G' above G'') (Fig. S4†). 3-arm-PCL-MA and 2-arm-P((D,L)LA-*co*-CL)-MA inks however, displayed a G' above G'' along the entire experiment, before and after UV irradiation, showing a higher elastic component in the resin already before irradiation. This was ascribed to certain chain ordering in the liquid resins or to a partial cross-linking of the ink.

The G' after cross-linking of the formed films was 3 ± 0.4 and 4 ± 0.5 MPa, of 0.4 ± 0.2 and 1 ± 0.1 MPa and of 0.9 ± 0.1 and 1.1 ± 0.1 MPa for the 2- and 3-arm- P(D,L)LA-MA, PCL-MA and P((D,L)LA-*co*-CL)-MA materials (Fig. 3E), showing again a higher G' for materials presenting 3-arms than the 2-arm counterparts. The flexibility of this system allowed us to create materials with a wide range of mechanical properties which were well on the range of several soft tissues such as the arterial wall, hyaline cartilage or the skin.[23]

3.3 Tensile properties of 3D printed and cross-linked materials

The mechanical properties of the 3D printed 2- and 3-arm copolymers and UV cross-linked 2- and 3-arm homopolymers were tested under tension (Fig. 4). All materials showed a rather stiff and brittle response, without plastic deformation, as observed by the absence of a clear strain hardening or necking before sample rupture (Fig. 4A).

The 2-arm based polymer films displayed in all cases a lower Young's modulus than their 3-arm counterparts, although this was only significantly different for the P((D,L)LA-MA based inks, with values of 6.2 ± 2.6 MPa and 624.6 ± 58.7 MPa for 2- and 3-arm P((D,L)LA-MA, 4.5 ± 0.6 MPa and 7.2 ± 0.7 MPa for 2- and 3-arm PCL-MA and 8.4 ± 0.3 MPa and 9.7 ± 0.9 MPa for 2- and 3-arm P((D,L)LA-*co*-CL)-MA films (Fig. 4B). As expected, P((D,L)LA-MA films showed the highest stiffness and PCL-MA the lowest, with P((D,L)LA-*co*-CL)-MA films showing an intermediate response. Maximum stresses followed the same trend with values of 1.7 ± 0.8 MPa and 19.6 ± 3.7 MPa for 2- and 3-arm P((D,L)LA-MA films; 0.2 ± 0.1 MPa and 0.4 ± 0.2 MPa for 2- and 3-arm PCL-MA films and 1.1 ± 0.3 MPa and 0.9 ± 0.1 MPa for 2- and 3-arm P((D,L)LA-*co*-CL)-MA films, respectively (Fig. 4C).

The maximum strain measured followed the opposite trend, with elongation at breaks that were the highest for the 2-arm based inks as compared to their 3-arm counterparts, although this was only significantly different for P(D,L)LA-MA films. Again P(D,L)LA-MA films showed the highest elongation at break and PCL-MA the lowest, with P((D,L)LA-*co*-CL)-MA copolymers showing an intermediate behaviour. 2- and 3-arm P(D,L)LA-MA films showed an elongation at break of 38.9 ± 18.5% and 8.5 ± 1.3%, respectively; 2- and 3-arm PCL-MA films of 7.1 ± 2.4% and 6.6 ± 2.7%, respectively and 2- and 3-arm

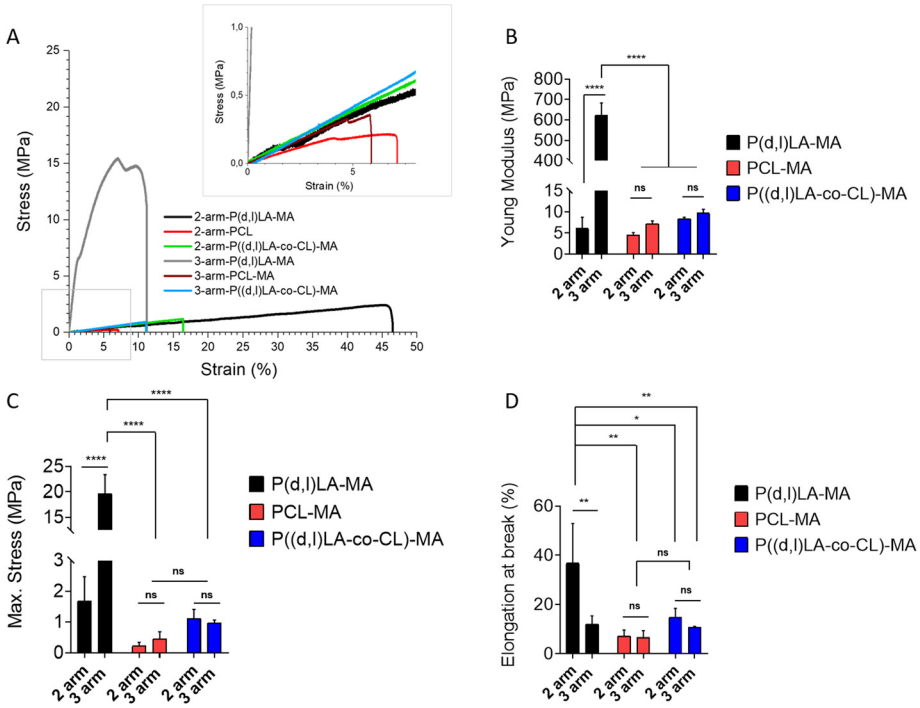

Fig. 4 Representative tensile test traces (A) of 2- and 3-arm copolymers and homopolymer films fabricated *via* 3D printing and UV cross-linking, respectively. Inset shows a zoom-in of the region labelled with a grey box. $n > 3$ for all samples. (B) Young's modulus, (C) maximum stress and (D) elongation at break calculated from tensile tests. Statistical significance was calculated from two-way ANOVA with Tukey's multiple comparison. For Young's modulus: test interaction $F(2,12) = 329.9$, $p < 0.0001$; arm number $F(1,12) = 336.3$, $p < 0.0001$; material type $F(2,12) = 329.3$, $p < 0.0001$. Adjusted p-values: $p < 0.1$ (ns), $p < 0.0322$ (*), $p < 0.0021$ (**), $p < 0.0002$ (***) and <0.0001 (****). For maximum stress: interaction $F(2,12) = 65.48$, $p < 0.0001$; arm number $F(1,12) = 66.37$, $p < 0.0001$; material type $F(2,12) = 81.43$, $p < 0.0001$. Adjusted p-values: $p < 0.1$ (ns), $p < 0.0322$ (*), $p < 0.0021$ (**), $p < 0.0002$ (***) and <0.0001 (****). For elongation at break: interaction $F(2,12) = 5.230$, $p = 0.0233$; arm number $F(1,12) = 8.738$, $p = 0,0120$; material type $F(2,12) = 9.613$, $p = 0,0032$. Adjusted p-values: $p < 0.1$ (ns), $p < 0.0322$ (*), $p < 0.0021$ (**), $p < 0.0002$ (***) and <0.0001 (****).

P((D,L)LA-*co*-CL)-MA films of 14.8 ± 3.4% and 10.7 ± 0.3%, respectively.

Melchels *et al.* synthesised P(D,L)-LA based resins using ethyl lactate as non-reactive diluent.[20] They investigated the impact of the number of arms (2-, 3- or 6-arm) of the synthesised resin on the mechanical properties of the prepared films by 3-point bending mechanical analysis. In contrast to our results, no relationship between the number of arms and the mechanical properties was observed. However, they observed a clear decrease in the flexural modulus with increasing molecular weight of the inks, that ranged from 2.5 to 3.6 GPa, approximately. Moreover, the resulting films were brittle, as expected for PLA-based inks, with the maximum elongation at break of 6.2% approximately. Similarly, Elomaa *et al.* prepared resins from PCL oligomers with molecular weights ranging from 800 to 6000 g mol^{-1} and showed a clear decrease of the tensile Young's modulus from 15 to 6.7 MPa with increasing molecular weight, which appear to be well on the range of the PCL based homopolymers synthesised here.[15] As expected, PCL based films accounted for an elongation at break higher than that reported for P(D,L)-LA based resins, with values ranging from 19 to 78% that were lowest for lower molecular weight inks.

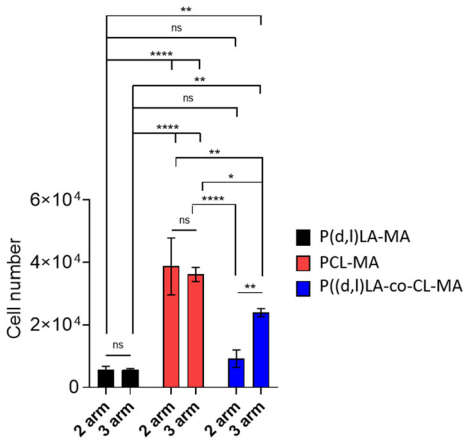

Fig. 5 hMSC adhesion after 24 h of culture on 2- and 3-arm-P(D,L)LA-MA, PCL-MA and P((D,L)LA-*co*-CL)-MA polymer films. Error bars represent standard deviation; n = 3. Statistical significance was calculated from two-way ANOVA with Tukey's multiple comparison test. For complex viscosity: interaction $F(2,12)$ = 8.049, p = 0.0061; arm number $F(1,12)$ = 4.558, p = 0.054; material type $F(2,12)$ = 95.62, p < 0.0001. Adjusted p-values: p < 0.1 (ns), p < 0.0322 (*), p < 0.0021 (**), p < 0.0002 (***) and <0.0001 (****).

3.4 Biocompatibility and cell adhesion support of the cross-linked materials

In order to evaluate the applicability of the synthesised inks as tissue engineering scaffolds and cell culture platforms, their capability to support cell adhesion and survival was tested *in vitro* with human bone marrow mesenchymal stem cells (hMSCs). hMSCs are known to readily respond to differences in their chemical and mechanical environment, making them ideal candidates to evaluate biocompatibility, adhesion and growth on novel materials.[24,25] To do so, films of the different resins were fabricated by DLP printing, in the case of 2- and 3-arm-P((D,L)LA-*co*-CL) copolymers, and *via* casting and UV cross-linking in the case of 2- and 3-arm-PCL-MA and P(D,L)LA-MA polymers. Cell–material interactions are a key parameter determining the integration of biomaterial scaffolds. The first step towards guiding cell processes through material interactions is the adhesion to the materials' surface. Analysis of the material's capability to support cell adhesion (Fig. 5) showed that after 24 h of culture PCL-MA films supported the highest cell adhesion with a total of 38 709 ± 9100 and 36 164 ± 2203 cells per film for 2- and 3-arm polymers, respectively. P(D,L)LA-MA showed the poorest cell adhesiveness with a total of 5643 ± 1000 and 5603 ± 388 cells per film for 2- and 3-arm polymers. PLA is known to display poor cell adhesion due to the hydrophobicity of its surface that limits the absorption of growth factors and proteins (and hence, cells) and multiple strategies have been developed to introduce negative charges through functionalization or formation of surface radicals.[26–28] Moreover, previously reported comparative studies of PLA and PCL polymers demonstrate the highest cell attachment supported by PCL-based materials.[29] 2- and 3-arm copolymers showed a behavior intermediate of that of the two homopolymers, with attached cell numbers of 9115 ± 2846 and 23 928 ± 1304 for 2- and 3-arm-P((D,L)LA-*co*-CL)-MA copolymers, respectively. Interestingly, this intermediate behavior made evident a higher cell attachment when the resins presented 3- instead of 2-arms, probably due to the higher storage modulus of the materials.

After initial adhesion (generally within 4 h), cells continue sensing their microenvironment and can adopt various cell morphologies and orientations, a process in which the substrate mechanical properties and topographical features play an important role.[30,31] Cell observation *via* fluorescence microscopy revealed that, despite having a higher number of adhere cells, hMSCs cultured in PCL-MA films for 24 h presented a rounded morphology together with the formation of large cell aggregates, suggesting that cell–cell interactions were stronger than cell–material interactions (Fig. 6). Cells cultured in P(D,L)LA-MA films, however, presented an elongated and well-spread morphology in both, 2-arm and 3-arm-based polymer films, which could be ascribed to the higher mechanical properties of the substrates (Fig. 3E and 4). Cells cultured on P((D,L)LA-*co*-CL)-MA copolymers presented a cell morphology that was intermediate to the observed for the two homopolymers. In fact, hMSCs cultured on 2-arm copolymers displayed rounded cells forming aggregates, while hMSCs cultured on 3-arm-copolymers presented a morphology more similar to the observed in PCL-MA substrates, with higher cell spread areas. After 24 h, cells cultured in all ink types were mostly viable with few cells dead, as demonstrated by the live/dead stain with red cells denoting compromised membranes and green stain showing live cells (Fig. 6B and Fig. S5†).

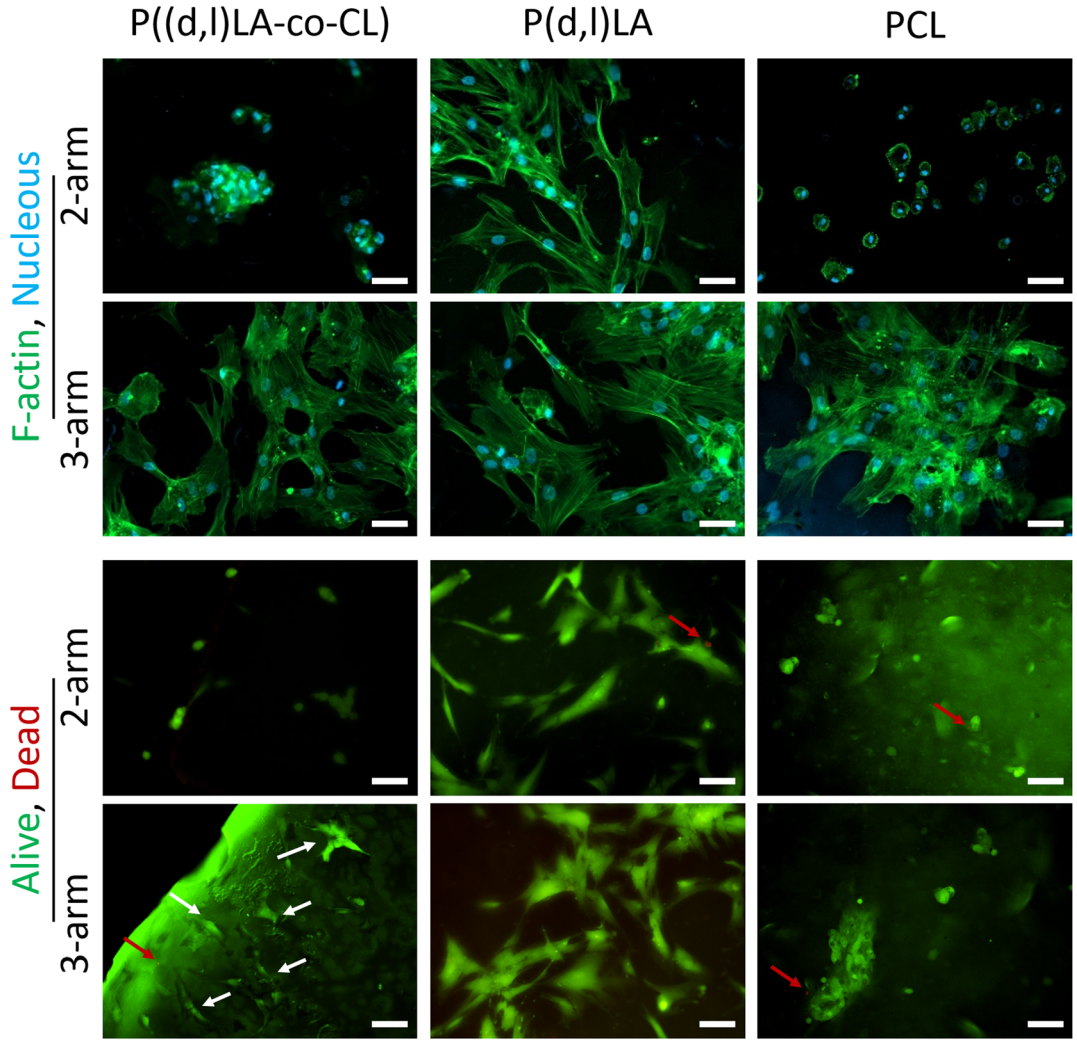

Fig. 6 Fluorescence microscopy images of hMSCs after 24 h of culture in homopolymer and copolymer films. (A) Morphology of the cells stained for F-actin (green, cytoskeleton) and nuclear DNA (blue, nucleus). Scale bar is 50 μm. (B) Live/Dead images of hMSCs stained for ethidium homodimer (red, dead), and calcein (green, alive). Scale bar is 50 μm.

3.5 Shape fidelity in DLP printed topographies

After proving the biocompatibility of (P(D,L)LA-*co*-CL)-MA inks, the shape fidelity post printing was evaluated. Shape fidelity is dependent on the printing resolution, cross-linking efficiency and structural stability of the fabricated objects.[3] For DLP printing and SLA techniques, the printing resolution is determined by the equipment (theoretical) but, is affected by the absorbance and scattering of light by the ink and the diffusion of radicals within the resin. To this end, light blockers that absorb light at the irradiation wavelength and limit scattering are very often included in the ink mixture. However, the inclusion of such molecules compromises the biocompatibility of the ink and supposes an extra component that can be released to the culture media when the fabricated structures are biodegradable. The cross-linking efficiency determines the light exposure time required to cross-link the object and the presence of unreacted species (monomers or prepolymers) in the final object. The latter affects the shape stability after washing and leaching the final object. This effect is further enhanced when non-reactive diluents are included in the reaction mixture, which will escape or leach during washing steps (or during culture in media).

The biocompatible P((D,L)LA-*co*-CL)-MA inks developed here were printed in the absence of light blockers and diluents, which facilitated shape stability after printing. A comparison between structures printed with reactive, non-reactive and without diluent revealed that the objects printed without diluent achieved a higher shape fidelity than those printed with diluent (Fig. S6 and Table S1†). Objects printed with reactive diluent presented also a good shape fidelity but, as explained earlier, included the reactive diluent in the final formulation which would alter the predesigned mechanical and chemical properties of the substrates.

To further investigate the achievable shape fidelity and resolution, repeating patterns of cubes, cylinders and cones

were fabricated *via* DLP printing (Fig. 7). Cubes and cylinders were designed to have dimensions of 300 × 300 μm (with × depth) and 300 μm diameter, respectively, with a constant height of 300 μm. The objects appeared to reproduce the designed pattern successfully across the entire surface of the chips, with printing errors lower than 21% in all dimensions (Table 2). Of note was that 3-arm-copolymers appeared to have an overall lower printing error than 2-arm-copolymers, probably due to the higher density of photoreactive groups. Fabrication of conical structures was designed with decreasing size, informing about the printing resolution of these challenging shapes. These structures usually require to set a gradient of exposure times that decreases as the height of the cone increases and the printed circle decreases in size. Hence, the highest error measured was for the height of the cones, reaching values as high as 126 ± 3% for the smallest printed cones. Indeed, the height printing error increased with decreasing size of the printed cone and was again smallest for the topographies printed with the 3-arm copolymer. Nevertheless, further optimization of the printing parameters would yield lower errors. The printing error at the base of the cones was much smaller than that of the height, with errors that ranged from 2–19% and increased again with the smaller cone sizes.

Table 2 Printing error of cube and pillar micro-topographies. ε_w: average error in the width of cubes; ε_h: average error in the height; $\varepsilon_\varnothing$: average error in the diameter of the cylinders and at the base of the cones; all calculated from SEM images

	Cubes		Cylinders		Cones	
	2-arm	3-arm	2-arm	3-arm	2-arm	3-arm
ε_w (%) ± SD	15 ± 14	12 ± 11	—	—	—	—
$\varepsilon_\varnothing$ (%) ± SD	—	—	21 ± 15	9 ± 7	2 ± 1 Cone 1 5 ± 1 Cone 2 19 ± 7 Cone 3	5 ± 2 Cone 1 8 ± 1 Cone 2 5 ± 7 Cone 3
ε_h (%) ± SD	21 ± 4	5 ± 4	11 ± 4	9 ± 5	35 ± 0.4 Cone 1 57 ± 1 Cone 2 126 ± 3 Cone 3	35 ± 1 Cone 1 42 ± 1 Cone 2 75 ± 23 Cone 3

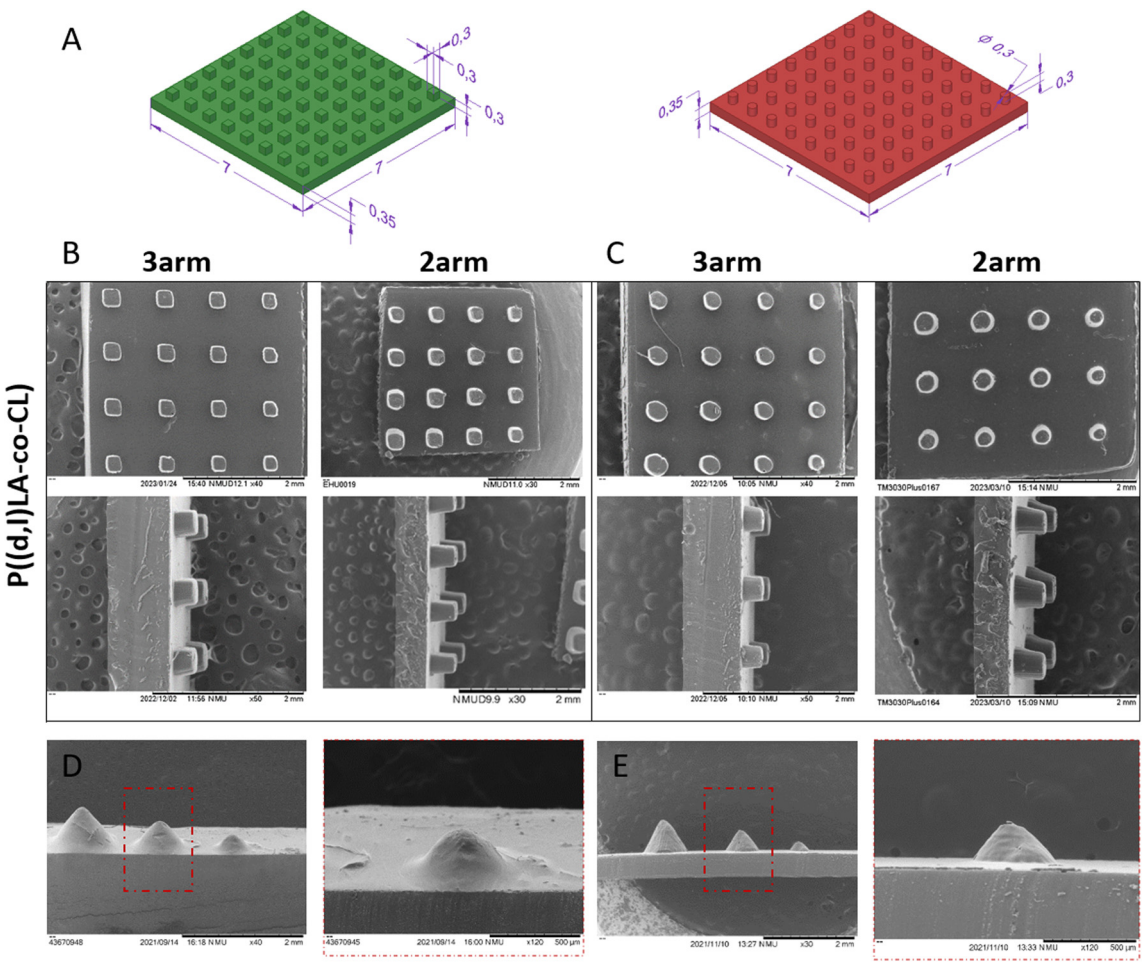

Fig. 7 (A) Computational design and dimensions of micro-topography models with cubes (left) and cylinders (right). (B and C) SEM images of top-view (top) and cross-view (bottom) of micro-topography using 3-arm- (left) and 2-arm-P((D,L)LA-*co*-CL) (right) as printable resins: (B) cube- and (C) pillar-surface structures were shown. Scale bar is 2 mm in all images. (D and E) SEM images of cones on gradient structures printed with 3-arm- (D) and 2-arm-P((D,L)LA-*co*-CL)-MA (E). Scale bars of 2 mm and 500 μm are shown in the left and right images, respectively.

4 Conclusions

Here, we report the synthesis of a library of P(D,L)LA and PCL-based low molecular weight homopolymer and copolymer inks with 2- and 3-arms. Methacrylation of the polymers yielded 2- and 3-arm-PCL-MA, P(D,L)LA-MA and P((D,L)LA-*co*-CL)-MA with high degrees of methacrylation that enabled a fast photocross-linking of the resins in 1–2 s. Analysis of the viscoelastic properties demonstrated that 3-arm PCL-MA, P(D,L)LA-MA, P((D,L)LA-*co*-CL)-MA and 2-arm-P((D,L)LA-*co*-CL)-MA accounted for a low viscosity and met the main requirements to be used in DLP printing, that is to behave as Newtonian fluids with a viscosity <10 Pa s. 2- and 3-arm-P((D,L)LA-*co*-CL)-MA copolymers were selected for DLP printing as they presented the lowest viscosities (1.4 ± 0.2 and 0.72 ± 0.05 Pa s). We showed that these inks were printable at room temperature and without the use of diluents, resulting in structures with higher shape fidelity and resolution as compared to prints of the same inks using non-reactive diluents. The inks were exploited to print micro-topographies in the shape of cubes, cylinders and cones, showing printing errors that decreased with increasing number of arms in the copolymer. Analysis of the biocompatibility and cell adhesion of the resulting materials showed that the materials supported hMSC adhesion and viability. hMSCs cultured in P((D,L)LA-*co*-CL)-MA copolymer films presented an intermediate behaviour to that of cells cultured in PCL-MA and P(D,L)LA-MA films. PCL-MA films showed the highest cell adhesion followed by P((D,L)LA-*co*-CL)-MA and P(D,L)LA-MA films. The apparent cell spread area appeared to be highest in P(D,L)LA-MA films, followed by P((D,L)LA-*co*-CL)-MA and PCL-MA films. Being hMSCs highly sensitive to their chemical, structural and mechanical microenvironment and having shown good biocompatibility to the developed materials, extrapolation of these resuls to other cell and tissue types is expected. Altogether, these data demonstrate the synthesis of novel DLP biocompatible inks that can be processed at room temperature and in a solvent free environment, yielding high resolution objects that could be further exploited as cell culture platforms or tissue engineering scaffolds. Extrapolation of these findings to 3D architectures for cell immunomodulation would be an interesting possibility as it would allow for precise control of sizes and topographies up to a scale that could enable cell polarization on command.

Author contributions

Sandra Ramos-Díez and Garazi Larrañaga-Jaurrieta contributed equally to this work: methodology, investigation, writing, visualization and formal analysis. Leire Iturriaga: Methodology and investigation. Ander Abarrategi: Supervision, writing and funding acquisition. Sandra Camarero-Espinosa: Conceptualization, methodology, investigation, supervision, writing, visualization, formal analysis and funding acquisition.

Conflicts of interest

There are no conflicts to declare.

Acknowledgements

The authors acknowledge the funding bodies and support through the EMAKIKER grant. S. C.-E. acknowledges the Spanish Ministry of Science and Innovation (MICINN) – State Investigation Agency (AEI) (PID2020-114901RA-I00). S. C.-E. and S. R.-D. acknowledge the Basque Government (PIBA_2022_1_0006). G. L.-J. acknowledges the Basque Government Predoctoral grant PRE_2021_1_0403. S. C.-E. and L. I. acknowledge the Provincial Council of Guipuzcoa. The project that gave rise to these results received the support of a fellowship from the "laCaixa" Foundation (ID100010434). The fellowship code is 117145. S. C.-E. acknowledges funding from the University of the Basque Country UPV/EHU within the framework of Grupos de Investigación (GIU21/033). A. A. acknowledges funding from PID2021-127191OB-I00 and RTI2018-101708-A-I00 funded by MCIN/AEI/10.13039/501100011033 and by "ERDF A way of making Europe". Grant RYC2018-025502-I funded by MCIN/AEI/10.13039/501100011033 and by "ESF Investing in your future".

References

1 L. Moroni, T. Boland, J. A. Burdick, C. De Maria, B. Derby, G. Forgacs, J. Groll, Q. Li, J. Malda, V. A. Mironov, C. Mota, M. Nakamura, W. Shu, S. Takeuchi, T. B. F. Woodfield, T. Xu, J. J. Yoo and G. Vozzi, *Trends Biotechnol.*, 2018, **36**, 384–402.
2 C. Mota, S. Camarero-Espinosa, M. B. Baker, P. Wieringa and L. Moroni, *Chem. Rev.*, 2020, **120**, 10547–10607.
3 A. Schwab, R. Levato, M. D'Este, S. Piluso, D. Eglin and J. Malda, *Chem. Rev.*, 2020, **120**, 11028–11055.
4 T. Duda and L. V. Raghavan, *IFAC-PapersOnLine*, 2016, **49**, 103–110.
5 Z. Chen, Z. Li, J. Li, C. Liu, C. Lao, Y. Fu, C. Liu, Y. Li, P. Wang and Y. He, *J. Eur. Ceram. Soc.*, 2019, **39**, 661–687.
6 P. N. Bernal, P. Delrot, D. Loterie, Y. Li, J. Malda, C. Moser and R. Levato, *Adv. Mater.*, 2019, **31**, 1904209.
7 P. N. Bernal, M. Bouwmeester, J. Madrid-Wolff, M. Falandt, S. Florczak, N. G. Rodriguez, Y. Li, G. Größbacher, R.-A. Samsom, M. van Wolferen, L. J. W. van der Laan, P. Delrot, D. Loterie, J. Malda, C. Moser, B. Spee and R. Levato, *Adv. Mater.*, 2022, **34**, 2110054.
8 K. S. Lim, J. H. Galarraga, X. Cui, G. C. J. Lindberg, J. A. Burdick and T. B. F. Woodfield, *Chem. Rev.*, 2020, **120**, 10662–10694.
9 D. Xue, J. Zhang, Y. Wang and D. Mei, *ACS Biomater. Sci. Eng.*, 2019, **5**, 4825–4833.
10 S. H. Kim, Y. K. Yeon, J. M. Lee, J. R. Chao, Y. J. Lee, Y. B. Seo, M. T. Sultan, O. J. Lee, J. S. Lee, S.-i. Yoon,

I.-S. Hong, G. Khang, S. J. Lee, J. J. Yoo and C. H. Park, *Nat. Commun.*, 2018, **9**, 1620.

11 H. Goodarzi Hosseinabadi, D. Nieto, A. Yousefinejad, H. Fattel, L. Ionov and A. K. Miri, *Appl. Mater. Today*, 2023, **30**, 101721.

12 A. Thomas, I. Orellano, T. Lam, B. Noichl, M.-A. Geiger, A.-K. Amler, A.-E. Kreuder, C. Palmer, G. Duda, R. Lauster and L. Kloke, *Acta Biomater.*, 2020, **117**, 121–132.

13 S. Pal and S. K. Asha, *Macromol. Chem. Phys.*, 2022, **223**, 2200139.

14 J. Jansen, F. P. W. Melchels, D. W. Grijpma and J. Feijen, *Biomacromolecules*, 2009, **10**, 214–220.

15 L. Elomaa, S. Teixeira, R. Hakala, H. Korhonen, D. W. Grijpma and J. V. Seppälä, *Acta Biomater.*, 2011, **7**, 3850–3856.

16 N. Paunović, J. Marbach, Y. Bao, V. Berger, K. Klein, S. Schleich, F. B. Coulter, N. Kleger, A. R. Studart, D. Franzen, Z. Luo and J.-C. Leroux, *Adv. Sci.*, 2022, **9**, 2200907.

17 B. J. Green, K. S. Worthington, J. R. Thompson, S. J. Bunn, M. Rethwisch, E. E. Kaalberg, C. Jiao, L. A. Wiley, R. F. Mullins, E. M. Stone, E. H. Sohn, B. A. Tucker and C. A. Guymon, *Biomacromolecules*, 2018, **19**, 3682–3692.

18 T. Kuhnt, R. Marroquín García, S. Camarero-Espinosa, A. Dias, A. T. ten Cate, C. A. van Blitterswijk, L. Moroni and M. B. Baker, *Biomater. Sci.*, 2019, **7**, 4984–4989.

19 Y. Bao, N. Paunović and J.-C. Leroux, *Adv. Funct. Mater.*, 2022, **32**, 2109864.

20 F. P. W. Melchels, J. Feijen and D. W. Grijpma, *Biomaterials*, 2009, **30**, 3801–3809.

21 T. Kuhnt, F. L. C. Morgan, M. B. Baker and L. Moroni, *Addit. Manuf.*, 2021, **46**, 102102.

22 R. Wang, F. Damanik, T. Kuhnt, A. Jaminon, S. Hafeez, H. Liu, H. Ippel, P. J. Dijkstra, N. Bouvy, L. Schurgers, A. T. ten Cate, A. Dias, L. Moroni and M. B. Baker, *Adv. Healthcare Mater.*, 2023, 2202648.

23 F. H. Silver and D. L. Christiansen, in *Biomaterials Science and Biocompatibility*, ed. F. H. Silver and D. L. Christiansen, Springer New York, New York, NY, 1999, pp. 187–212, DOI: 10.1007/978-1-4612-0557-9_7.

24 A. J. Engler, S. Sen, H. L. Sweeney and D. E. Discher, *Cell*, 2006, **126**, 677–689.

25 S. Camarero-Espinosa and J. J. Cooper-White, *Biomaterials*, 2019, **210**, 105–115.

26 M. Schroepfer, F. Junghans, D. Voigt, M. Meyer, A. Breier, G. Schulze-Tanzil and I. Prade, *ACS Omega*, 2020, **5**, 5498–5507.

27 B. N. Teixeira, P. Aprile, R. H. Mendonça, D. J. Kelly and R. M. d. S. M. Thiré, *J. Biomed. Mater. Res., Part B*, 2019, **107**, 37–49.

28 R. A. Quirk, W. C. Chan, M. C. Davies, S. J. B. Tendler and K. M. Shakesheff, *Biomaterials*, 2001, **22**, 865–872.

29 S. Camarero-Espinosa and L. Moroni, *Nat. Commun.*, 2021, **12**, 1031.

30 A. D. Doyle and K. M. Yamada, *Exp. Cell Res.*, 2016, **343**, 60–66.

31 J. Zonderland and L. Moroni, *Biomaterials*, 2021, **268**, 120572.

